PHYSICAL REVIEW C VOLUME 28, NUMBER 4 OCTOBER 1983

Hypernuclear excitation through kaon photoproduction

Shian S. Hsiao and Stephen R. Cotanch
Department of Physics, North Carolina State University, Raleigh, North Carolina 27650
(Received 7 January 1983)

The Λ hypernuclear spectrum excited in the weakly interacting electromagnetic production process $A(\gamma,K^+)_\Lambda B$ is theoretically surveyed. Plane wave impulse approximated multiple-scattering calculations for hypernuclear formation from ^{4}He, ^{12}C, and ^{208}Pb targets are presented for a wide range of lab and excitation energies. Excitation energies and transition densities are calculated within a lambda-particle, proton-hole model using Woods-Saxon basis wave functions. The transition operator is constructed using the free (bare) amplitudes for the elementary process $\gamma+p\rightarrow K^+ +\Lambda$ which are evaluated from Feynman diagrams including both strange meson (K,K*) and baryon (Λ,Σ) exchange. These amplitudes are dominated by Λ and scalar K exchange; however, effects from Σ and vector K* exchange are found to be significant even near threshold. The hypernuclear selective excitation is documented in detail for $\theta=0°$. Transitions to unnatural parity states and substitutional states with medium to high spin are predicted to be strong. Because of large momentum transfer (≥ 200 MeV/c), the (γ,K) reaction is highly quasielastic and a low, roughly 0.1, Λ "sticking probability" is estimated using an approximate hypernuclear sum rule. The excitation process is sensitive to the interior as cross section calculations for $^{208}\mathrm{Pb}(\gamma,K^+)^{208}_{\ \Lambda}\mathrm{Tl}$ involving bound Λ 1s, 2s, and 3s configurations, unrestricted by the Pauli exclusion principle, reveal markedly different signatures. Cross section sensitivity is also investigated and discussed for off-shell amplitude effects, variations in the Λ-nucleus spin-orbit interaction, and different sets of phenomenological coupling constants which equivalently describe the $\gamma+p\rightarrow K^+ +\Lambda$ process. Finally, estimates for electroproduction, $A(e,e'K^+)_\Lambda B$, are also presented and discussed. Both photoproduction and electroproduction cross sections are calculated to be measurably large for the beam energies, 1 to 3 GeV, of proposed intense electron accelerators.

NUCLEAR REACTIONS Kaon photoproduction and Λ hypernuclear formation. Theoretical survey of $\sigma(E_{\mathrm{lab}},E_x)$ for $^4_\Lambda$H, $^{12}_{\ \Lambda}$B, and $^{208}_{\ \Lambda}$Tl. Plane wave impulse approximation and particle-hole wave functions. Investigation of cross section sensitivity to theoretical uncertainties. Application of hypernuclear sum rule. Electroproduction hypernuclear cross section estimates.

I. INTRODUCTION

Although hypernuclei were discovered[1] thirty years ago, it has only been in the last decade that hypernuclear physics has emerged as a developing field attracting significant international attention.[2] This transition has been fostered by both impressive state-of-the-art experimental advances and by the growing awareness of the importance of meson and quark degrees of freedom in the nucleus. The presence of a strange baryon, such as a Λ or Σ particle, inside the nucleus provides an exciting opportunity to study an exotic system. In addition to the novelty, investigating hypernuclei will facilitate improvements in conventional many-body nuclear theory and, as important, will provide new information concerning elementary particles and their interactions. For example, it may be possible to determine whether the Λ lifetime is extended or even shortened[3] in the nuclear medium.

The current work addresses the subject of hypernuclei from a nuclear structure viewpoint and focuses on the excitation of Λ hypernuclear states through the photoproduction reaction $A(\gamma,K^+)_\Lambda B$. Initial calculations for this process have been reported by Bernstein, Donnelly, and Epstein.[4] We extend their treatment and further document the utility of this reaction: a soft reasonably understood electromagnetic component combined with the weakly interacting K^+ and mildly interacting Λ which is not constrained by the Pauli principle. As demonstrated below, the (γ,K^+) reaction preferentially excites unnatural parity hypernuclear states, and thereby compliments the more strongly absorbing processes (K^-,π^-) (Ref. 5) and (π^+,K^+) (Ref. 6) which selectively excite natural parity states. We also investigate the interior probing capability of the (γ,K^+) reaction by examing the cross section sensitivity to the unrestricted Λ orbital quantum numbers. We find distinct signatures for different Λ orbitals used to describe the same final state. Finally, we estimate electroproduction cross sections for the reaction $A(e,e'K^+)_\Lambda B$ and compare them with our photoproduction results to provide additional motivation for an intense high energy electron accelerator which recently has been proposed.[7]

This paper, for which preliminary results have been previously reported,[8–10] is organized into five sections. In Sec. II we calculate the amplitude for the elementary process $\gamma+\mathrm{p}\rightarrow\mathrm{K}^++\Lambda$ from Feynman diagrams involving hyperon exchange. The fundamental coupling constants are obtained from the earlier work of Thom[11] which we reproduce and confirm. Much of our discussion in this section is contained and further amplified in Ref. 11. The elementary amplitudes are essential ingredients needed for computing the hypernuclear formation cross section. As described in Sec. III, our procedure for constructing the formation cross section is similar to the "first generation" pion photoproduction calculations[12–14] which used first-order multiple scattering theory and the impulse approximation. Although improved theoretical meson photoproduction treatments now exist,[15] our approach should be sufficient for the present feasibility study and does extend our earlier investigations,[9,10] as well as the calculations reported by the MIT group,[4,16] by including the full kaon production operator and more realistic wave functions. In Sec. IV we apply our formalism to the closed shell targets ^{4}He, ^{12}C, and ^{208}Pb and present survey calculations for a wide range of beam and excitation energies to document the probing capability and selective excitation aspects of the (γ,K^+) reaction. Finally, we summarize our findings in Sec. V.

II. ELEMENTARY KAON PHOTOPRODUCTION

Consider the associated strangeness photoproduction process

$$\gamma+\mathrm{p}\rightarrow\mathrm{K}^++\Lambda\ .$$

The invariant cross section[17] for this reaction induced by photons having polarization vector $\hat{\epsilon}_\lambda(\lambda=\pm1)$ is $(\hbar=c=1)$

$$d\sigma=(2\pi)^4\frac{|\sqrt{E_\gamma E_{\mathrm{N}}}t^\lambda\sqrt{E_{\mathrm{K}}E_\Lambda}|^2\delta^4(p_{\mathrm{K}}+p_\Lambda-p_\gamma-p_{\mathrm{N}})d\vec{k}_{\mathrm{K}}d\vec{k}_\Lambda}{[(p_\gamma\cdot p_{\mathrm{N}})^2-p_\gamma^2p_{\mathrm{N}}^2]^{1/2}E_{\mathrm{K}}E_\Lambda}\ , \tag{1}$$

where the energy E, momentum $\vec{k}$, and four-vector $p=(E,\vec{k})$ $(p^2=M^2,\ M=\text{mass})$ are, respectively, labeled γ, N, K, and Λ to represent the photon, proton, K^+ meson, and lambda particle. The transition amplitude t^λ is related to the S-matrix element S^λ by the usual expression,

$$S^\lambda=2\pi i\delta^4(p_{\mathrm{K}}+p_\Lambda-p_\gamma-p_{\mathrm{N}})t^\lambda\ , \tag{2}$$

and is given in terms of Dirac spinors $u(p)$ by[11,17]

$$t^\lambda=\frac{1}{(2\pi)^4}\left[\frac{M_\Lambda M_{\mathrm{N}}}{4E_\gamma E_{\mathrm{N}}E_{\mathrm{K}}E_\Lambda}\right]^{1/2}\bar{u}(p_\Lambda)\sum_{j=1}^{4}A_j\mathcal{M}_j^\lambda u(p_{\mathrm{N}})\ . \tag{3}$$

The gauge and Lorentz invariant matrices $\mathcal{M}_j$ can be represented in terms of the Dirac matrices $\gamma=(\gamma_0,\vec{\gamma})$, γ_5, and momentum four-vectors

$$\mathcal{M}_1^\lambda=-\gamma_5\gamma\cdot\epsilon_\lambda\gamma\cdot p_\gamma\ , \tag{4a}$$

$$\mathcal{M}_2^\lambda=2\gamma_5(\epsilon_\lambda\cdot p_{\mathrm{N}}p_\gamma\cdot p_\Lambda-\epsilon_\lambda\cdot p_\Lambda p_\gamma\cdot p_{\mathrm{N}})\ , \tag{4b}$$

$$\mathcal{M}_3^\lambda=\gamma_5(\gamma\cdot\epsilon_\lambda p_\gamma\cdot p_{\mathrm{N}}-\gamma\cdot p_\gamma\epsilon_\lambda\cdot p_{\mathrm{N}})\ , \tag{4c}$$

$$\mathcal{M}_4^\lambda=\gamma_5(\gamma\cdot\epsilon_\lambda p_\gamma\cdot p_\Lambda-\gamma\cdot p_\gamma\epsilon_\lambda\cdot p_\Lambda)\ . \tag{4d}$$

Here $\epsilon_\lambda=(0,\hat{\epsilon}_\lambda)$ is the photon's polarization four-vector. The spin-independent amplitudes A_j, also gauge and Lorentz invariant, can be computed directly from Feynman diagrams (see Fig. 1). These amplitudes, which are functions of the Mandelstam variables and the fundamental coupling constants, are completely specified in the Appendix of Ref. 11.

Figure 1 summarizes the Feynman diagrams considered in the current work. Strange meson exchange (K, scalar coupling; K*,[18] vector and tensor coupling) as well as Λ and Σ baryon exchange are included in the nonresonant description of the elementary photoproduction process. Contributions from baryon resonances are omitted but will be examined in a future study. The vertex parameters naturally group into four effective coupling constants which can be phenomenologically adjusted to reproduce the data

$$g_\Lambda=g_{\mathrm{K}\Lambda\mathrm{N}}\ , \tag{5a}$$

$$G_\Sigma=k_Tg_{\mathrm{K}\Sigma\mathrm{N}}\ , \tag{5b}$$

$$G_V=g_{\mathrm{K}^*\mathrm{K}\gamma}g^V_{\mathrm{K}^*\Lambda\mathrm{N}}\ , \tag{5c}$$

$$G_T=g_{\mathrm{K}^*\mathrm{K}\gamma}g^T_{\mathrm{K}^*\Lambda\mathrm{N}}\ . \tag{5d}$$

The remaining constants in Fig. 1 are the fundamental charge e and proton (μ_{p}), lambda (μ_Λ), and transition (μ_T) moments which are also specified in Ref. 11. Table I lists

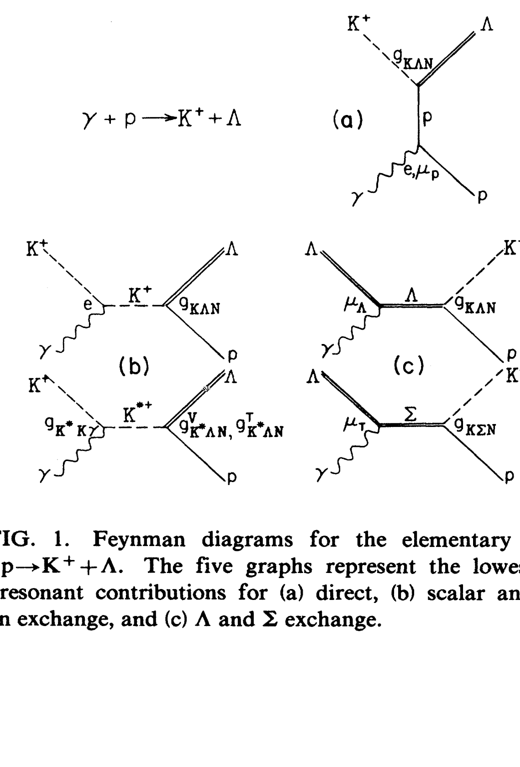

FIG. 1. Feynman diagrams for the elementary reaction $\gamma+\mathrm{p}\rightarrow\mathrm{K}^++\Lambda$. The five graphs represent the lowest order, nonresonant contributions for (a) direct, (b) scalar and vector kaon exchange, and (c) Λ and Σ exchange.

TABLE I. Effective coupling constants for the reaction $\gamma+p\rightarrow K^+=\Lambda$.

	$\frac{g_\Lambda}{(4\pi)^{1/2}}$	$\frac{G_\Sigma}{(4\pi)^{1/2}}$	$\frac{G_V}{4\pi}$	$\frac{G_T}{4\pi}$
Set 1	2.57	1.52	0.105	0.064
Set 2	2.49	1.16	0.226	−0.062

two independent sets of effective coupling constants determined[11] by an empirical analysis of $K\Lambda$ photoproduction cross section and polarization data.

Using these parameters and the above equations we have reproduced the work of Ref. 11. Figure 2 is a representative result verifying that both solutions describe the data. We have also studied the relative contribution to the production process from each meson and baryon exchange. Figure 3 illustrates the dominance of K and Λ exchange in the zero degree lab cross section. Notice that including Σ and K^* exchange is also significant. It should be stressed that the coupling constants in Table I are appropriate for the energy region covered in Ref. 11, threshold to 1.4 GeV. We have compared predictions with available data at higher energies and find reasonable agreement at forward angles ($\theta \leq 30°$). For these angles the differential cross section for solution set 1 agrees to within 5% over the energy interval 1.05 to 2.2 GeV but overpredicts by a factor of 2 in the region 3.4 to 4.1 GeV. However, even at 5 GeV predictions for extreme forward angles ($\theta < 12°$) only average 1.5 times larger than experiment. For this same energy region, solution set 2 provides poorer agreement, since predictions are generally 50% larger than solution set 1, except near 0° where solutions from the two sets are essentially equal. Further, both sets of solutions significantly overestimate the total cross section at higher energies. However, because only the 0° amplitude enters our hypernuclear formation calculations, our predictions using solution set 1 should be adequate for energies at or below the 2 to 3 GeV region. Our higher energy predictions will probably be too large and therefore should be regarded as rough estimates awaiting corrections from an improved description of the elementary amplitudes.

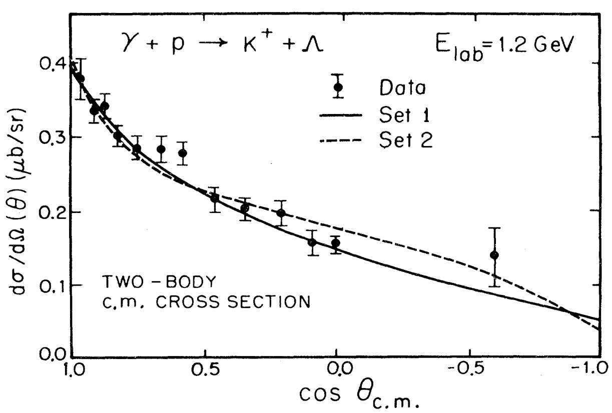

FIG. 2. Comparison of the theoretical and experimental c.m. cross section for $\gamma+p\rightarrow K^++\Lambda$ at $E=1.2$ GeV. The theoretical curves represent two independent sets of empirical coupling constants.

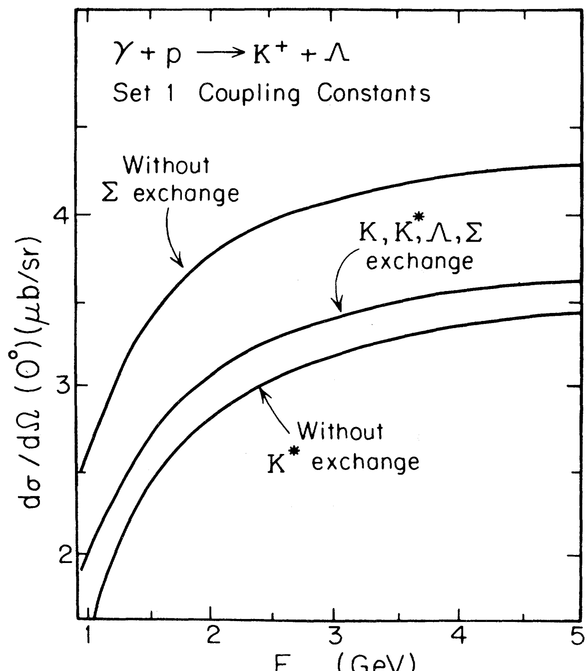

FIG. 3. Theoretical zero-degree lab cross section for $\gamma+p\rightarrow K^++\Lambda$ for energies up to 5 GeV. The center curve represents the full solution while the top and bottom curves, respectively, represent the effects of Σ and K^* exchange.

In the next section we construct the hypernuclear formation amplitude using the impulse approximation and the elementary on-shell amplitudes discussed above. Because our many-body wave functions are specified in terms of Pauli spinors, χ_s ($s=$ N or Λ magnetic spin component), it is convenient to introduce an effective production operator $v^\lambda(\vec{k}_\gamma)$ by the relation

$$t^\lambda\delta(\vec{k}_K+\vec{k}_\Lambda-\vec{k}_\gamma-\vec{k}_N)\equiv\langle\chi_\Lambda,\vec{k}_\Lambda;\vec{k}_K\,|\,v^\lambda(\vec{k}_\gamma)\,|\,\vec{k}_N,\chi_N\rangle\ , \tag{6}$$

which involves plane waves and Pauli spinors having normalization

$$\langle\vec{k}\,|\,\vec{k}'\rangle=\delta(\vec{k}-\vec{k}')\ ,$$

$$\langle\chi_s\,|\,\chi_{s'}\rangle=\delta_{ss'}\ .$$

Combining Eqs. (3) and (6) yields

$$v^\lambda(\vec{k}_\gamma)=a(E_\gamma)\frac{e^{-i\vec{k}_\gamma\cdot\vec{r}}}{(2\pi)^{3/2}}\vec{\sigma}\cdot\hat{\epsilon}_\lambda\delta(\vec{r}-\vec{r}')\ , \tag{7}$$

where $\vec{\sigma}$ is the baryon Pauli spin operator and $a(E_\gamma)$ is a linear combination of the Feynman amplitudes A_j. This combination depends upon the Lorentz frame and is specified in the next section.

III. HYPERNUCLEAR FORMATION AMPLITUDE

The thrust of this work is to present a realistic, theoretical survey of hypernuclear excitation through the reaction

$$\gamma + A \to K^+ + {}_\Lambda B ,$$

where one of the Z protons in the target nucleus A is converted into a lambda particle forming the hypernucleus $B \equiv {}_\Lambda B$. Equation (1) also gives the cross section for this process with the substitutions $N \to A$, $\Lambda \to B$, and $t^\lambda \to T^\lambda$. The formation amplitude T^λ can be computed using the nuclear wave functions and the exact, many-body multiple-scattering operator τ^λ which describes the elementary production in the nuclear medium. For 0^+ targets and final hypernuclear states $|j_B m_B\rangle$, we have

$$T^\lambda \delta(\vec{k}_K + \vec{k}_B - \vec{k}_\gamma - \vec{k}_A) = \langle j_B m_B, \vec{k}_B; \vec{k}_K | \tau^\lambda | \vec{k}_A, 0 \rangle , \tag{8}$$

where the final state vector is a product of kaon and hypernuclear wave functions. The many-body nuclear and hypernuclear state vectors have unit normalization.

Invoking the factorized impulse approximation we replace τ^λ with the sum of Z effective operators $v^\lambda(\vec{k}_\gamma)$, defined above, which describe free on-shell production from each target proton. We also use the frozen nucleon approximation and compute all formation cross sections in the target laboratory frame (i.e., $\vec{k}_A = \vec{k}_N = 0$). Combining Eqs. (3), (4), and (7) yields the on-shell elementary amplitude coefficient for zero-degree kaons,

$$a(E_\gamma) = \left[\frac{k_\gamma e'_\Lambda}{8E'_K E'_\Lambda} \right]^{1/2} \left[\left[\frac{k'_\Lambda}{e'_\Lambda} - 1 \right] A_1 + M_N A_3 + (E'_\Lambda - k'_\Lambda) A_4 \right] , \tag{9}$$

with

$$e'_\Lambda = E'_\Lambda + M_\Lambda .$$

The prime indicates that k'_Λ and k'_K are determined by conserving energy and momentum for the elementary reaction $\gamma + p \to K^+ + \Lambda$ in the proton's rest frame. It is important not to confuse these values with the unprimed momenta appearing in the phase space expression for the hypernuclear formation cross section. Unprimed quantities, in particular k_K and k_Λ, represent the physical momenta in the many-body lab frame ($\vec{k}_A = 0$). This point is addressed further in the next section where we examine off-shell effects for this reaction.

Substituting Eq. (7) into Eq. (8) and using second quantized notation for the photoproduction operator, which is a one-body operator in the space of the target nucleons, we obtain

$$T^\lambda(\vec{q}) = \frac{a(E_\gamma)}{(2\pi)^3} \sum_{\mu,\nu} I^\lambda_{\nu\mu} \langle j_B m_B | b^\dagger_\nu a_\mu | 0 \rangle , \tag{10}$$

where $\vec{q}$ is the momentum transferred to the hypernucleus,

$$\vec{q} = \vec{k}_\gamma - \vec{k}_K ,$$

and

$$I^\lambda_{\nu\mu} = \langle \phi_\nu | e^{-i\vec{q}\cdot\vec{r}} \vec{\sigma}\cdot\hat{e}_\lambda | \phi_\mu \rangle \tag{11}$$

is a matrix element involving standard single-particle radial and spin-angle functions with unit normalization

$$\phi = \frac{u_{nlj}(r)}{r} \mathscr{Y}^m_{lj}(\hat{r}, \vec{\sigma}) . \tag{12}$$

The subscripts ν and μ represent the quantum numbers $\{n, l, j, m\}$ for the Λ and N, respectively. The Λ creation operator $b^\dagger_\nu$ commutes with the N annihilation operator a_μ since these particles are distinguishable.

The final approximation concerns the kaon, target nucleus, and hypernucleus wave functions. We use plane waves for the kaon and consider only closed shell targets. Particle-hole wave functions are adopted for the final state. We do not diagonalize the Λ-N interaction; however, we plane to examine configuration mixing in the future.[19] Again utilizing the Fock formalism we have, for fixed initial $\beta = \{n_N, l_N, j_N, m_N\}$ and final $\alpha = \{n_\Lambda, l_\Lambda, j_\Lambda, m_\Lambda\}$ single-particle states,

$$|j_B m_B\rangle = \sum_{m_N m_\Lambda} (-1)^{j_N - m_N} \times C(j_N j_\Lambda j_B, -m_N m_\Lambda m_B) b^\dagger_\alpha a_\beta | 0 \rangle . \tag{13}$$

Substituting Eq. (13) into Eq. (10) and applying Wick's theorem yields for the zero-degree formation amplitude

$$T^\lambda(0^\circ) = \frac{a(E_\gamma)}{(2\pi)^3} \sum_{m_N m_\Lambda} (-1)^{j_N - m_N} \times C(j_N j_\Lambda j_B, -m_N m_\Lambda m_B) I^\lambda_{\alpha\beta} . \tag{14}$$

The matrix element $I^\lambda_{\alpha\beta}$ can be evaluated by standard angular momentum techniques. Decomposing the operator into multipoles we have

$$e^{-i\vec{q}\cdot\vec{r}} \vec{\sigma}\cdot\hat{e}_\lambda = -(2\pi)^{1/2} \sum_{j \geq 1} (-i)^j \hat{j} (\lambda \Sigma^\lambda_j + i \Sigma'^\lambda_j) , \tag{15}$$

with $\hat{j} = \sqrt{2j+1}$. The magnetic, Σ^λ_j, and electric, Σ'^λ_j, multipoles are, respectively,

$$\Sigma^\lambda_j = \vec{X}^\lambda_{jj} \cdot \vec{\sigma} , \tag{16}$$

$$\Sigma'^\lambda_j = \frac{j^{1/2}}{\hat{j}} \left[-\vec{X}^\lambda_{jj+1} + \left[\frac{j+1}{j} \right]^{1/2} \vec{X}^\lambda_{jj-1} \right] \cdot \vec{\sigma} , \tag{17}$$

where the vector operator $\vec{X}^\lambda_{jl}$ is given in terms of the spherical Bessel functions $j_l(qr)$,

$$\vec{X}^\lambda_{jl} = j_l(qr) \sum_{m\mu} C(l\,1j, m\mu\lambda) \mathscr{Y}^m_l(\hat{r}) \hat{e}_\mu . \tag{18}$$

The spherical unit vectors are defined by

$$\hat{e}_{\pm 1} = \mp(\hat{e}_x \pm i\hat{e}_y)/\sqrt{2}, \quad \hat{e}_0 = \hat{e}_z ,$$

and the Condon and Shortly phase convention is adopted for the Clebsch-Gordan coefficients, $C(j_1j_2j_3,m_1m_2m_3)$, and spherical harmonics, $\mathscr{Y}_l^m$. Combining Eqs. (5)–(18), applying the Wigner-Eckart theorem, and performing the magnetic summations produces

$$T^{\lambda}=\frac{(-1)^d}{(2\pi)^{5/2}}a(E_\gamma)\delta_{\lambda m_B}\langle\Lambda||(\lambda\Sigma_{j_B}+i\Sigma'_{j_B})||\mathrm{N}\rangle \quad (19)$$

with phase specified by $d=j_\Lambda+j_\mathrm{N}+j_B/2+1$. The reduced matrix elements ($\Lambda\equiv n_\Lambda l_\Lambda j_\Lambda$, $\mathrm{N}\equiv n_\mathrm{N} l_\mathrm{N} j_\mathrm{N}$) can be directly evaluated using

$$\langle\Lambda||\vec{X}_{j_Bl}\cdot\vec{\sigma}||\mathrm{N}\rangle=(-1)^{l_\Lambda}\left[\frac{3}{2\pi}\right]^{1/2}\hat{l}_\mathrm{N}\hat{j}_\mathrm{N}\hat{l}_\Lambda\hat{j}_\Lambda\hat{l}\hat{j}_B C(l_\Lambda l l_\mathrm{N},000)\begin{Bmatrix} l_\Lambda & l_\mathrm{N} & l \\ \frac{1}{2} & \frac{1}{2} & 1 \\ j_\Lambda & j_\mathrm{N} & j_B\end{Bmatrix} I_l\,, \quad (20)$$

involving the standard nine-j coefficient and integral over the single-particle radial wave functions

$$I_l=\int_0^\infty u_\Lambda^*(r)j_l(qr)u_\mathrm{N}(r)dr\,. \quad (21)$$

Finally, combining Eqs. (1) and (19) we obtain the zero-degree lab cross section averaged over the incident photon polarization and summed over final hypernuclear spin orientations,

$$\frac{d\sigma}{d\Omega}(0^\circ)=C[\,|\langle||\Sigma_{jB}||\mathrm{N}\rangle|^2+|\langle\Lambda||\Sigma'_{jB}||\mathrm{N}\rangle|^2]\,, \quad (22)$$

with

$$C=\frac{a(E_\gamma)^2k_\mathrm{K}E_\mathrm{K}}{2\pi(1-qE_\mathrm{K}/k_\mathrm{K}E_B)}\,. \quad (23)$$

Because our calculations treat a specific single-baryon transition to a final hypernuclear state with spin j_B only one of the two reduced matrix elements contributes. Unnatural parity states $\pi_B=(-1)^{j_B+1}$ involve pure electric multipoles, while excitation of natural parity hypernuclear states $\pi_B=(-1)^{j_B}$ utilizes magnetic multipoles. The complete selection rules are given by

$$\vec{j}_B=\vec{j}_\Lambda+\vec{j}_\mathrm{N}=\vec{l}+\vec{1}\,,$$

$$\vec{l}=\vec{l}_\Lambda+\vec{l}_\mathrm{N}\,,$$

$$\pi_B=(-1)^{l_\Lambda+l_\mathrm{N}}=(-1)^l\,,$$

$$T_B=T_A+\tfrac{1}{2}\,,$$

where T_A and T_B specify the target and hypernuclear isospins.

IV. RESULTS

We have calculated formation cross sections for the three closed-shell targets ^{4}He, ^{12}C, and ^{208}Pb leading to the respective hypernuclei $^4_\Lambda$H, $^{12}_\Lambda$B, and $^{208}_\Lambda$Tl. The excitation energies and particle-hole wave functions were constructed using single-particle eigenvalues and eigenfunctions generated by a Woods-Saxon potential of the form

$$V(r)=f(r)+\frac{\lambda_{so}}{45.2}\vec{l}\cdot\vec{s}\,\frac{1}{r}\frac{df}{dr}(r)\,,$$

with

$$f(r)=\frac{V_0}{1+e^{(r-R)/a}}$$

and

$$R=r_0A^{1/3}\,.$$

The potential parameters, strengths V_0 and λ_{so}, radius r_0, and diffuseness a are listed in Table II. Table III summarizes the predicted single-particle eigenvalues for all bound states in the three nuclear systems.

The $^{12}_\Lambda$B excitation spectrum for all (1p-1h) hypernuclear states involving bound 1s and 1p Λ orbitals is presented in Fig. 4. The relative excitation strength, computed for 2.0 GeV incident photons, is indicated as a fraction of the ground state $(1s_{1/2},\,1s_{1/2}^{-1})_{1^+}$ cross section. Solid lines represent calculations using Woods-Saxon radial wave functions while dashed lines represent the same calculation but now using harmonic oscillator wave functions. We use the oscillator parameter 1.78 fm reported in the MIT study[16] and have reproduced their work as a check on both calculations.

Notice the significant differences in the excitation spectrum between harmonic oscillator and Woods-Saxon wave functions. The use of Woods-Saxon wave functions enhances the lambda 1s cross sections but reduces the weakly bound lambda 1p cross sections. The 0.62 scale factor in Fig. 4 is the required renormalization of the $(1s_{1/2},\,1s_{1/2}^{-1})_{1^+}$ Woods-Saxon cross section needed for absolute value agreement with the $(1s_{1/2},\,1s_{1/2}^{-1})_{1^+}$ harmonic oscillator result.

Figure 5 presents a limited survey of hypernuclear formation cross sections in terms of energy and target mass number. Theoretical lab cross sections, using set 1 elementary coupling constants, are plotted for specific unnatural parity states in $^4_\Lambda$H, $^{12}_\Lambda$B, and $^{208}_\Lambda$Tl for lab photon energies from threshold to 5 GeV. For comparison the elementary lab cross section (dashed line), multiplied by 0.2 for illustrative convenience, is also plotted. The signi-

TABLE II. Baryon-nucleus potential parameters.

	V_0 (MeV)	λ_{so} (fm)^2	r_0 (fm)	a_0 (fm)
Proton	-60.0	18.0	1.25	0.6
Lambda	-30.0	0.0	1.10	0.6

TABLE III. Predicted signal-baryon separation energies.

	$^{208}_{\Lambda}$Tl		$^{12}_{\Lambda}$B		$^{4}_{\Lambda}$H	
nlj	p	Λ	p	Λ	p	Λ
$1s_{1/2}$	−34.2	−25.85	−30.2	−10.1	−13.8	−1.6
$1p_{3/2}$	−30.9	−21.7	−13.8	−0.1		
$1p_{1/2}$	−30.6	−21.7	−9.5	−0.1		
$1d_{5/2}$	−26.5	−16.9				
$1d_{3/2}$	−25.75	−16.9				
$2s_{1/2}$	−23.0	−15.3				
$1f_{7/2}$	−21.3	−11.4				
$1f_{5/2}$	−20.0	−11.4				
$2p_{3/2}$	−17.0	−9.2				
$2p_{1/2}$	−16.4	−9.2				
$1g_{9/2}$	−15.4	−5.5				
$1g_{7/2}$	−13.2	−5.5				
$2d_{5/2}$	−10.0	−3.2				
$2d_{3/2}$	−8.9	−3.2				
$1h_{11/2}$	−9.7	−0.1				
$3s_{1/2}$	−7.8	−2.6				

ficance of Fig. 5 is that at 2 GeV the predicted hypernuclear formation cross section is measurably large, about 0.5 μb. This is roughly $\frac{1}{5}$ of the elementary cross section.

Figure 6 highlights an interesting result which relates to the interior probing capability of the (γ,K^+) process. The three curves correspond to different numbers of modes in the Λ s-wave radial wave function. The Λ node sensitivity is large and should be present in more elaborate calculations[19] including kaon distortions, Fermi motion, and off-shell effects. It may be possible to use the (γ,K^+) reaction to learn more about the nuclear interior through low-lying orbitals which are not restricted by the Pauli exclusion principle.

The final four figures, Figs. 7—10, document the selective excitation aspects in kaon photoproduction. Our pre-

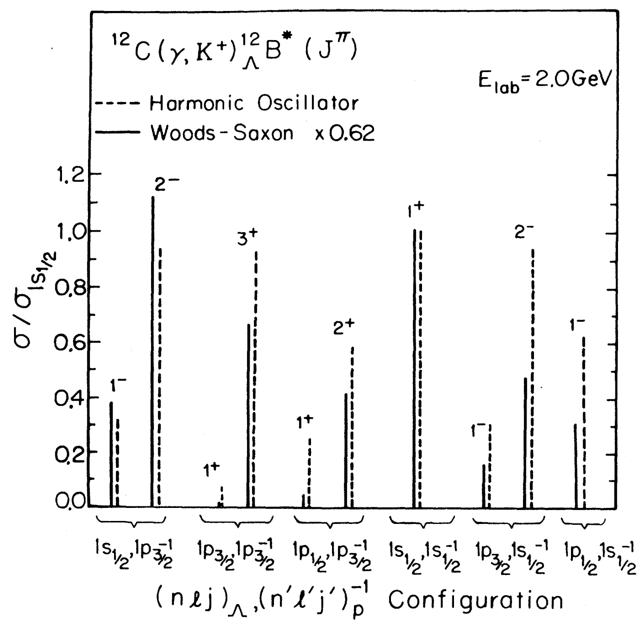

FIG. 4. Bound excitation spectrum for ^{12}B. Relative lab zero-degree cross sections are normalized to the $(1s_{1/2},\ 1s_{1/2}^{-1})_{1^+}$ ground state for Woods-Saxon (solid bars) and harmonic oscillator (dashed bars) single-particle wave functions. The absolute Woods-Saxon cross section must be multiplied by 0.62 to equal the harmonic oscillator prediction for the $(1s_{1/2},\ 1s_{1/2}^{-1})_{1^+}$ state.

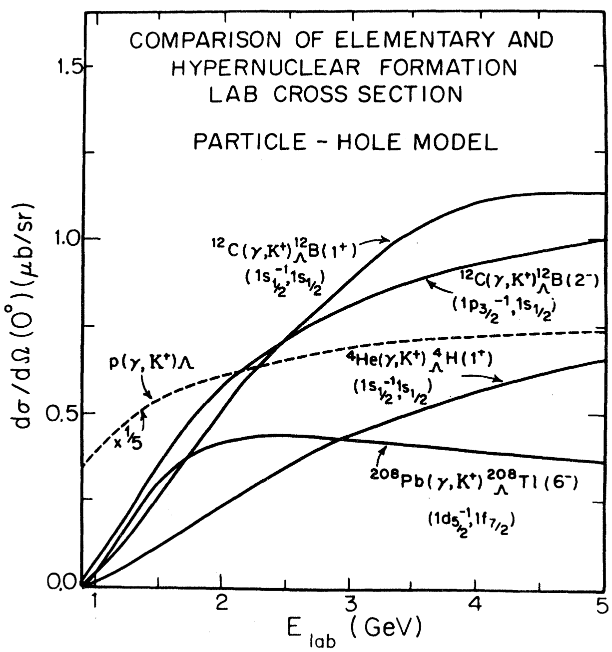

FIG. 5. Zero-degree hypernuclear formation cross section for ^{4}He, ^{12}C, and ^{208}Pb targets. Dashed curve represents the zero-degree elementary lab cross section, multiplied by 0.2 for illustrative convenience.

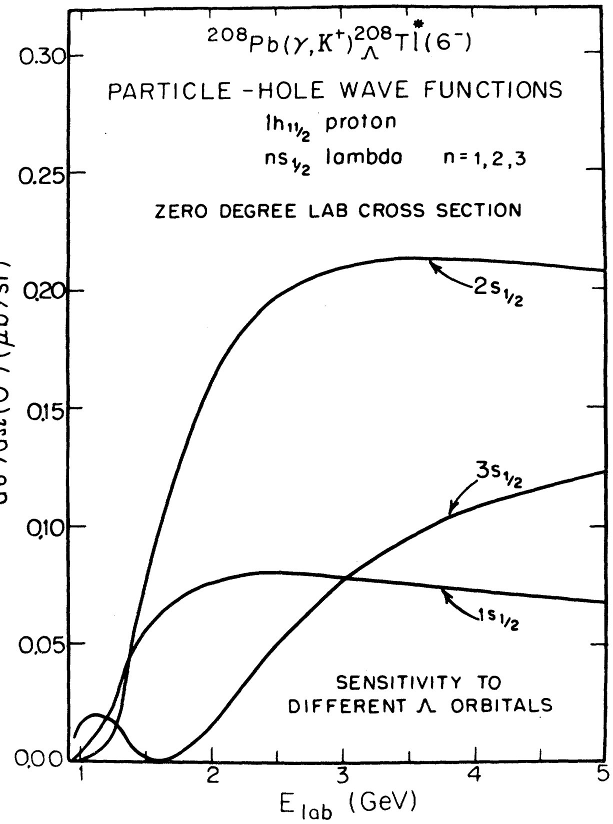

FIG. 6. Hypernucleus cross section sensitivity to Λ single-particle wave function. The three curves represent identical calculations using $1s_{1/2}$, $2s_{1/2}$, and $3s_{1/2}$ Λ radial wave functions.

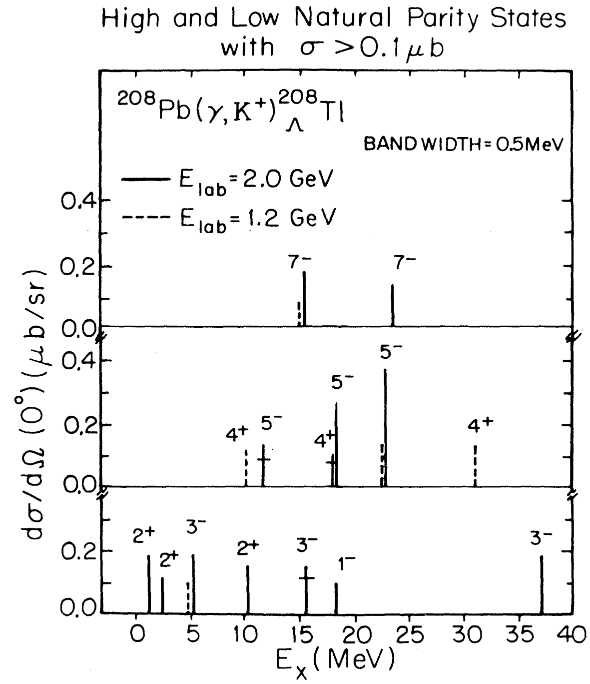

FIG. 8. Low and high spin, natural parity spectrum predicted for $^{208}_{\Lambda}$Tl. Only states with lab cross sections larger than 0.1 μb are indicated. The excitation energy is computed using the single-particle energies summarized in Table III. Cross sections for states having the same spin but different configurations have been added if their excitation energies are within 0.5 MeV. These "complexes" are indicated by horizontal marks.

dictions are for the reaction ^{208}Pb $(\gamma,K^+)^{208}_{\Lambda}$Tl at energies 1.2 GeV (dashed lines) and 2.0 GeV (solid lines). The distribution of strength for the substitutional states (p→Λ in the same orbital configuration) is illustrated in Fig. 7.

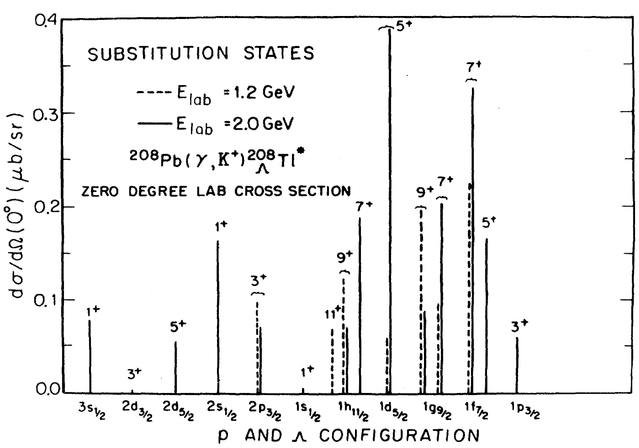

FIG. 7. Dominant substitution states predicted for $^{208}_{\Lambda}$Tl. For each Λ and p single-particle configuration (identical) the largest cross section and corresponding final spin parity is represented. In this figure, as in Figs. 8–10, cross sections are plotted for $E_{\text{lab}} = 1.2$ GeV (dashed lines) and 2.0 GeV (solid lines).

Medium and high spin states are preferentially excited. In Figs. 8–10 we have indicated the excitation energy and strength of all 1p-1h states excited in $^{208}_{\Lambda}$Tl which have cross sections greater than 0.1 μb and excitation energies less than 40 MeV. Notice that unnatural parity states dominate the spectrum. This is expected since, as Eqs. (16) and (17) indicate, the unnatural parity transition operator $\Sigma_j'^{\lambda}$ is more effective in transferring linear and angular momentum than is the natural parity transition operator Σ_j^{λ}. Also notice that high spin states are more strongly excited at 1.2 GeV than at 2.0 GeV while the reverse is true for low spin states. This can be understood from the monotonic decrease of the momentum transfer q with increasing energy and the property of the spherical Bessel functions $[j_l(qr)$ peaks for $l \simeq j_B \simeq qR]$ governing the radial integrals [Eq. (21)].

The physical hypernuclear excitation spectrum will not exactly resemble our predictions. The true states have a natural width and overlap, especially at higher energies. Limitations introduced by experimental resolution compound this effect and generate a spectrum characterized by groups or complexes of states. With this in mind we have combined all predicted states having the same spin and parity that are separated by less than $\frac{1}{2}$ MeV. The presence of "theoretical" complexes are represented by horizontal bars in Figs. 8–10. The use of improved structure wave functions may also introduce further

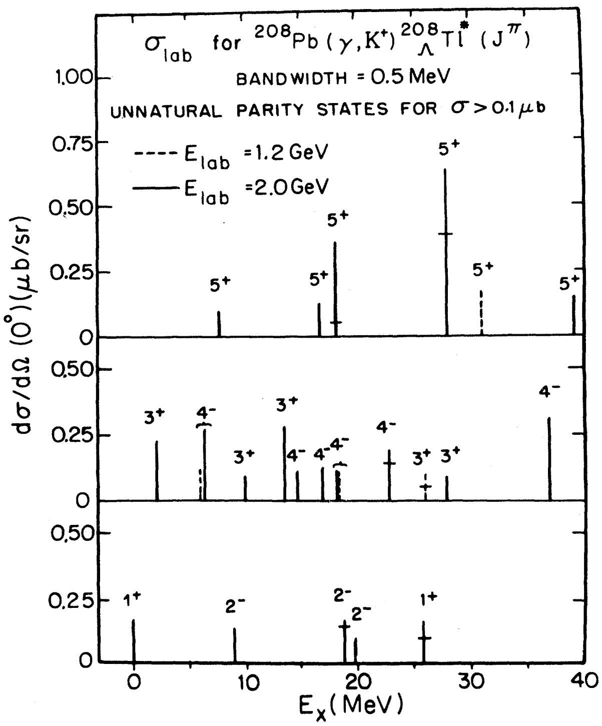

FIG. 9. Same as Fig. 8 for low to medium spin unnatural parity states.

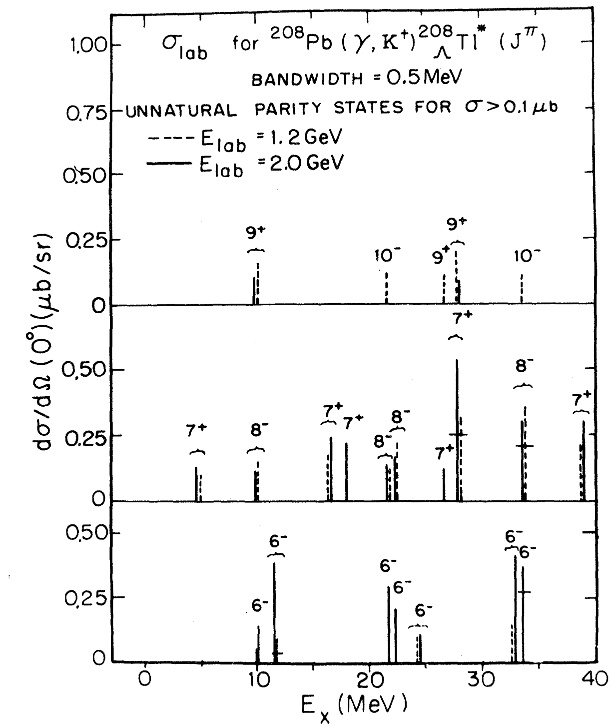

FIG. 10. Same as Fig. 8 for medium to high spin unnatural parity states.

changes. The diagonalization of the ΛN interaction, even though relatively weak, can in certain situations[20,21] lead to significant mixing and redistribution of excitation strength. This correction will be included in future calculations.[19] We conclude that all strongly excited states predicted in this work are logical candidates for mixing.

Another deficiency, common to all shell model calculations, is that our wave functions are not translationally invariant (spurious center of mass effects). If many-body harmonic oscillator wave functions are used this error can be corrected by simply multiplying the matrix element in Eq. (19) by $e^{-q^2b^2/4A}$ where b is the oscillator parameter. We have omitted this refinement and consider it to be more consistent with the next level of improved calculations that include kaon distortions. As is often true for independent corrections, these two effects tend to be offsetting since matrix elements will be reduced by distortions and increased by the center-of-mass recoil correction. Further, because we use Woods-Saxon wave functions the choice in oscillator parameter is ambiguous. In any event, using the values[16] $b=1.34$ for ^{4}He and 1.70 for ^{12}C we estimate that the matrix elements would be enhanced by a factor of 1.34 for ^{4}He and 1.16 for ^{12}C at 1.2 GeV. At 2 GeV the respective corrections are 1.20 and 1.10. This effect, being of order $1/A$, is negligible for ^{208}Pb.

We briefly summarize other studies which have been conducted. We estimate that for both light and heavy targets the (γ,K) process is predominantly quasielastic and quasiinelastic. This conjecture is based upon an approximate energy independent sum rule. Following Dalitz and Gal[22] we sum the plane wave cross section Eq. (22) over all final hypernuclear states f (both bound and in the continuum) and invoke closure to yield

$$\sum_f \frac{d\sigma^f}{d\Omega}(0°,\gamma A \to \mathrm{K}^+ B) = Z\frac{d\sigma}{d\Omega}(0°,\gamma p \to \mathrm{K}^+\Lambda) \ . \quad (24)$$

Quasielastic and quasiinelastic processes generally produce unbounded Λ particles described by continuum wave functions. The probability for this occurrence is the complement to the Λ "sticking probability." From Eq. (24) the latter is given by Z_{eff}/Z where the effective proton number is

$$Z_{\mathrm{eff}} = \frac{\displaystyle\sum_{f \in b} \frac{d\sigma^f}{d\Omega}(0°,\gamma A \to \mathrm{K}^+_\Lambda B)}{\displaystyle\frac{d\sigma}{d\Omega}(0°,\gamma p \to \mathrm{K}^+\Lambda)} \ , \quad (25)$$

and the sum is over only the bound state spectrum. We have estimated Z_{eff} by computing $d\sigma^f/d\Omega$ for all 1p-1h bound states (about 60 significant levels for $^{208}_{\Lambda}$Tl). Table IV lists our results for the hypernuclei $^4_\Lambda$H, $^{12}_\Lambda$B, and $^{208}_\Lambda$Tl at lab energies 1.2 and 2.0 GeV. The low Λ sticking probabilities are associated with the high momentum transfer. Because q decreases with increasing energy more of the sum rule is exhausted at 2 GeV.

The plane wave hypernuclear sum rule, Eq. (24), can also be used to estimate kaon distortion effects. The dominant distortion effect is from absorption which, to first

TABLE IV. Λ sticking probabilities for the reaction $A(\gamma,K^+)_\Lambda B$.

B_Λ	$E_{lab}=1.2$ GeV	$E_{lab}=2.0$ GeV
${}^{4}_{\Lambda}H$	0.01	0.04
${}^{12}_{\Lambda}B$	0.06	0.13
${}^{208}_{\Lambda}Tl$	0.05	0.09

order, will reduce absolute cross sections but not appreciably alter cross section ratios. Computing the photoproduction cross section with kaon distorted waves $\psi(\vec{r})$ modifies the sum rule result by replacing the physical charge Z with Z_{DW} given by

$$Z_{DW}=\int |\psi(\vec{r})|^2\rho_c(r)d\vec{r} ,$$

where $\rho_c(r)$ is the target charge density normalized to Z. Plane wave cross sections are therefore renormalized by $F=Z_{DW}/Z<1$ leading to a reduction factor of $1-F$. Assuming that both the charge density and absorptive component of the kaon optical potential $W(r)$ are proportional to the matter density $\rho_m(r)$, we have

$$Z_{DW}=\frac{Z}{A}\frac{\rho_m(0)}{W(0)}|\psi(\vec{r})|^2W(r)d\vec{r} ,$$
$$=\frac{Z\lambda\sigma_R}{V} .$$

Here $V=A/\rho_m(0)$ is the target volume and λ is the kaon mean free path

$$\lambda=\frac{1}{\rho_m(0)\sigma_{KN}}$$
$$=\frac{\hbar v}{2W(0)}$$

involving the kaon velocity v and the average kaon-nucleon total cross section σ_{KN}. The quantity σ_R is the kaon nucleus reaction cross section

$$\sigma_R=\frac{2}{\hbar v}\int |\psi(\vec{r})|^2W(r)d\vec{r} ,$$

which simplifies in the optical limit of Glauber theory to

$$\sigma_R=2\pi\int_0^\infty(1-e^{-\chi(b)})b\,db ,$$

with

$$\chi(b)=\sigma_{KN}\int_{-\infty}^{\infty}\rho_m(r)dz .$$

For a uniform mass distribution of radius R we can exactly evaluate σ_R and obtain, for the renormalization factor,

$$F=\frac{3}{x^3}\left[\frac{x^2}{2}-1+(1+x)e^{-x}\right] ,$$

where x is the ratio of the nuclear diameter to the mean free path

$$x=\frac{2R}{\lambda} .$$

Using the value $r_0=1.25$ from Table II to compute R and $\rho_m(0)$ we have

$$x=0.3A^{1/3}\sigma_{KN} .$$

In our photoproduction calculations the kaon momentum varies from 0.5 to 4.8 GeV as the photon energy E_γ increases from 0.9 to 5 GeV. In this energy range the kaon-nucleon cross section increases from 12 mb to a peak of 18.5 mb at $E_\gamma=1.5$ GeV and then slowly decreases to about 17 mb over the remaining interval. For ${}^{12}C$ $F=0.75$ just above the production threshold and decreases to a minimum of 0.65 at $E_\gamma=1.5$ GeV. For ${}^{208}Pb$ F varies between 0.51 and 0.39 for this same energy interval. Summarizing, distortion effects should not be too large for light nuclei, roughly 30%. For heavy targets this effect becomes almost twice as important, between 50 and 60%, and should be included if accurate absolute cross sections are desired. Furthermore, since we utilize a sum rule to estimate distortion effects, we have obtained an averaged renormalization factor. For excitation of specific hypernuclear states, especially those involving a deeply bound Λ as in ${}^{208}Pb$, distortions could be even more important with renormalization factors perhaps as low as 0.1. Distorted wave calculations, which are in progress,[19] will provide definitive assessments of this effect.

We also have examined the sensitivity of the theoretical formation cross section to uncertainties in (1) the Λ spin-orbit interaction; (2) elementary coupling constants, and (3) off-shell and momentum dependence of the elementary amplitudes. For ${}^{208}_{\Lambda}Tl$ varying the Λ spin-orbit strength $\lambda_{so}\ V_0^\Lambda$ from 0 to $\frac{1}{3}$ of the proton value produces only small changes in the cross section, except for weakly excited states having cross sections less than 0.1 μb. Thus it may be necessary to examine the analyzing power (polarized photons) to learn more about the relatively weak Λ spin-orbit interaction.

Changing the fundamental coupling constants from set 1 to set 2 (see Table I) produced very small effects in the hypernuclear cross section. Cross sections differed by about 2% when averaged over the energy interval from threshold to 5 GeV.

The results from the off-shell study are more significant. Our calculation uses the on-shell amplitudes evaluated in the target rest frame. We have extrapolated the amplitude coefficient $a(E_\gamma)$ defined by Eq. (9) off shell by replacing primed kinematical quantities with corresponding unprimed values. The unprimed quantities are determined from energy-momentum conservation in the many-body frame. For the kaon p_K does not significantly differ from p'_K, however, p_Λ and p'_Λ may differ substantially due to the large momentum transfer. For consistency p_Λ was determined using the frozen baryon approximation which requires both the lambda and the outgoing hypernucleus to have the same lab velocity. With this prescription we computed the "off-shell" amplitude coefficient $a(E_\gamma)$ and new cross section. For the $(1s_{1/2},1p_{3/2}^{-1})_{2^-}$ in ${}^{12}_{\Lambda}B$ the cross section is significantly larger, between roughly a factor of 3.5 at threshold and about 2.0 at $E_{lab}=2.0$ GeV. Although this is a large effect, one should be cautious in concluding that off-shell effects are important in the (γ,K) reaction. Our off-shell

TABLE V. Electroproduction cross section estimates for several final hypernuclear states. Cross sections, in units nb/(GeV sr^2), are computed for three different sets of particle kinematics. Energies are in GeV's.

${}_{\Lambda}B((nlj)_N^{-1},\ (nlj)_{\Lambda})_{J^{\pi}}$	Set 1 $E_e=2.0$, $E_\gamma=1.0$ $\theta_{e'}=10°$	Set 2 $E_e=1.3$, $E_\gamma=1.2$ $\theta_{e'}=5°$	Set 3 $E_e=3.0$, $E_\gamma=2.0$ $\theta_{e'}=4.6°$
${}^{4}_{\Lambda}\mathrm{H}(1s_{1/2}^{-1},\ 1s_{1/2})_{1^+}$	0.22	2.04	7.78
${}^{12}_{\Lambda}\mathrm{B}(1s_{1/2}^{-1},\ 1s_{1/2})_{1^+}$	0.50	4.54	16.28
${}^{12}_{\Lambda}\mathrm{B}(1p_{3/2}^{-1},\ 1s_{1/2})_{2^-}$	1.09	7.71	18.13
${}^{208}_{\Lambda}\mathrm{Tl}(1d_{5/2}^{-1},\ 1f_{7/2})_{6^-}$	0.50	6.07	13.34
${}^{208}_{\Lambda}\mathrm{Tl}(1f_{7/2}^{-1},\ 1g_{9/2})_{8^-}$	10.14	9.79	5.98

prescription is ambiguous and incomplete since the invariant amplitudes A_1, A_3, and A_4 appearing in Eq. (9) have remained unchanged. Because they are functions of the elementary Mandelstam variables they also should be extrapolated off shell. A more detailed study including this effect will be reported in a future communication.[19] Careful documentation of the off-shell behavior is important in order to utilize this reaction to probe nuclear structure and also to learn more about the elementary process in ways that are not feasible in particle experiments.

Our final result concerns hypernuclear formation through kaon electroproduction, $A(\mathrm{e,e'K^+})_{\Lambda}B$. Calculations for the complete one photon (virtual) exchange cross section for this process are in progress. We wish to determine if this reaction can be used to study the longitudinal hypernuclear form factor (structure function) which does not enter the (γ,K) analysis. As a prelude to that investigation and also to provide further information for assessing the relative merits of (γ,K) versus (e,e'K) experiments, we present here approximate electroproduction cross section calculations for the three hypernuclei studied in this work. For a discussion of the experimental considerations, including count rate estimates and coincidence electroproduction measurements, consult the recent work by Bernstein.[23] In the limit of real photon kinematics (virtual photon's mass approaches zero) the electroproduction lab cross section σ^3 depends only on the transverse form factor and is proportional to the lab photoproduction cross section[24]

$$\sigma^3 \equiv \frac{d^3\sigma}{d\Omega_{e'} dE_{e'} d\Omega_K} = \frac{1}{2\pi^2}\frac{\alpha}{1-\epsilon}\frac{E_{e'}}{E_e}\frac{k_\gamma}{(E_\gamma^2-k_\gamma^2)}\frac{d\sigma}{d\Omega_K}(\gamma,\mathrm{K}) \ . \tag{26}$$

Here $\alpha=\frac{1}{137}$ is the fine structure constant and E_e and $E_{e'}$ are the electron's initial and final lab energies. The virtual photon's energy E_γ and momentum k_γ are no longer equal and independently satisfy

$$E_\gamma = E_e - E_{e'} \simeq k_e - k_{e'} \ ,$$
$$\vec{k}_\gamma = \vec{k}_e - \vec{k}_{e'} \ ,$$

where k_e and $k_{e'}$ are the electron's initial and final momentum. The quantity ϵ is a measure of the virtual photon's transverse linear polarization and in the limit of real photon kinematics $E_\gamma \to k_\gamma$ is given by

$$\frac{1}{1-\epsilon} \to 1 + 2\frac{k_e k_{e'}}{k_\gamma^2} \ .$$

Table V lists the electroproduction cross sections for exciting specific hypernuclear states in ${}^{4}_{\Lambda}$H, ${}^{12}_{\Lambda}$B, and ${}^{208}_{\Lambda}$Tl. The cross section for zero-degree kaons has been calculated for three different sets of electron kinematics: (1) $E_e=2.0$ GeV, $E_{e'}=1.0$ GeV, $\theta_{e'}=10°$; (2) $E_e=1.3$ GeV, $E_{e'}=0.1$ GeV, $\theta_{e'}=5°$; and (3) $E_e=3.0$ GeV, $E_{e'}=1.0$ GeV, $\theta_{e'}=4.6°$. These sets permit direct comparison to the electroproduction estimates of other investigators.[23,25,26] Set (1) is used in the Lee-Schiffer[25] work which reports for ${}^{12}_{\Lambda}$B $(1s_{1/2},\ 1s_{1/2}^{-1})_{1^+}$ $\sigma^3 \simeq 10^{-4}$ μb/(GeV sr^2) while set (2) is the choice used in the Fetisov *et al.* estimate[26] which predicts for ${}^{7}_{\Lambda}$He (ground state) $\sigma^3 \simeq 10^{-3}$ μb/(GeV sr^2). Bernstein[23] presents experimental considerations which favor set (3). His estimate for ${}^{12}_{\Lambda}$B $(1s_{1/2},\ 1s_{1/2}^{-1})_{1^+}$ is $\sigma^3 = 7.2\times10^{-3}$ μb/(GeV sr^2) with a corresponding kaon count rate of 27 counts/hour assuming a 50 μA electron current and a target thickness of 0.25 g/cm^2. Our results are similar to Bernstein's and we concur with his conclusion that coincidence experiments of the tagged photon or (e,e'K) type should be feasible using a 100% duty cycle electron accelerator.

V. CONCLUSION

The thrust of our work has been a theoretical survey of hypernuclear excitation through kaon photoproduction. In summary we predict the following: (1) measurable hypernuclear formation cross sections for a wide variety of energies, targets, and final excited states; (2) selective excitation of unnatural parity states; (3) a predominantly quasielastic nature for the (γ,K) reaction with an approximate Λ sticking probability of 0.1; (4) cross section sensitivity to different Λ single-particle orbitals but insensitivity to the Λ-nucleus spin-orbit interaction and the fundamental coupling constants; (5) excitation of medium to high spin states at high momentum ($E_{\mathrm{lab}} \simeq 1.2$ GeV) and low to medium spin states at lower momentum transfer ($E_{\mathrm{lab}} \simeq 2.0$ GeV); and (6) measurably large electroproduction cross section estimates.

Because kaon photoproduction is the weakest nuclear interaction involving a hadron it is the ideal probe for both nuclear and hypernuclear structure, especially for studying transition spin densities and unnatural parity states. The reaction mechanism is reasonably understood and is amenable to an accurate theoretical description. The only uncertainties concern the energy and off-shell behavior of the elementary amplitudes. For energies above 1.2 GeV it may be necessary to include contributions from baryon resonances.[11] It would also be useful to have a phenomenological analysis of the $\gamma+p\rightarrow K^{+}+\Lambda$ reaction for energies between 1.2 GeV and 3.0 GeV. Because of the large momentum transfer associated with the (γ,K) process off-shell effects may be significant and further detailed study is planned.[19] Other topics which we intend to investigate are Σ hypernuclei, a more exact electroproduction survey, and kaon photoproduction through strange quark pair creation. Owing to the weak absorption associated with kaon photoproduction a comparison of a quark versus a meson-baryon exchange picture may provide useful insight.

In conclusion, advancing the field of hypernuclear physics and obtaining a comprehensive understanding of hypernuclei will require extensive reaction analyses using the complementary excitation processes (K^{-},π^{-}), (π^{+},K^{+}), (γ,K^{+}), and $(e,e'K^{+})$. Experiments involving the purely hadronic reactions have already been performed and future experiments are expected.[3] However, no electromagnetic excitation experiments have been conducted since an intense high energy electron accelerator is necessary. In view of the many unique, attractive aspects of electroexcitation and photoexcitation and the significant potential of hypernuclear physics, proposals[7] for such a facility merit serious consideration.

ACKNOWLEDGMENTS

The authors wish to acknowledge support provided by the U. S. Department of Energy. Also acknowledged are useful discussions with A. M. Bernstein, T. W. Donnelly, R. H. Dalitz, F. Tabakin, and L. Ludeking.

[1]M. Danrsz and J. Pniewski, Philos. Mag. 44, 348 (1953).

[2]Proceedings of the International Conference on Hypernuclear and Kaon Physics, Heidelberg, 1982, edited by B. Povh. See also Proceedings of the International School of Intermediate Energy Nuclear Physics, Verona, Italy, 1981, edited by R. Bergere, S. Costa, and C. Schaerf.

[3]L. Kisslinger, see Ref. 2, p. 49.

[4]A. M. Bernstein, T. W. Donnelly, and G. N. Epstein, Proceedings of the Symposium on Perspectives in Electro- and Photo-nuclear Physics, Saclay, 1980.

[5]B. Povh. Annu. Rev. Nucl. Sci. 28, 18 (1978).

[6]C. B. Dover, L. Ludeking, and G. F. Walker, Phys. Rev. C 22, 2073 (1980).

[7]Future Directions in Electromagnetic Nuclear Physics, edited by P. Stoler, 1979; see also Argonne Reports Nos. ANL-PHY-79-2, 1979 and ANL-82-22, 1982.

[8]S. R. Cotanch, in *Proceedings of the Ninth International Conference on High Energy Physics and Nuclear Structure, Versailles, 1981,* edited by P. Catillon, P. Radvanyi, and M. Porneuf (North-Holland, Amsterdam, 1982), p. 367.

[9]S. Hsiao and S. R. Cotanch, Bull. Am. Phys. Soc. 27, 531 (1982).

[10]S. R. Cotanch and S. Hsiao, see Ref. 2, p. 327.

[11]H. Thom, Phys. Rev. 151, 1322 (1966).

[12]J. H. Koch and T. W. Donnelly, Nucl. Phys. B 64, 478 (1973).

[13]A. Nagl and H. Uberall, Phys. Lett. 63B, 291 (1976).

[14]G. N. Epstein, M. K. Singham, and F. Tabakin, Phys. Rev. C 17, 702 (1978).

[15]M. K. Singham, G. N. Epstein, and F. Tabakin, Phys. Rev. Lett. 43, 1476 (1979).

[16]A. M. Bernstein, T. W. Donnelly, and G. N. Epstein, Nucl. Phys. A358, 195 (1981).

[17]M. Gourdin and J. Dufour, Nuovo Cimento 27, 1410 (1963).

[18]T. K. Kuo, Phys. Rev. 129, 2264 (1963).

[19]S. Hsiao, L. Ludeking, and S. Cotanch (unpublished).

[20]E. H. Auerbach, A. J. Baltz, C. B. Dover, A. Gal, S. H. Kahana, L. Ludeking, and D. J. Millener, Phys. Rev. Lett. 47, 1110 (1981); S. H. Kahana (private communication).

[21]R. Sinha and A. K. Kerman (private communication).

[22]R. H. Dalitz and A. Gal, Phys. Lett. 64B, 154 (1976).

[23]A. M. Bernstein, see Ref. 2, p. 409.

[24]A. Donnachie, *High Energy Physics,* edited by E. H. J. Burhop (Academic, New York, 1972), Vol. V.

[25]J. Schiffer and T. S. H. Lee, Argonne National Laboratory Report ANL-82-83, 69, 1982; and private communication.

[26]V. N. Fetisov, M. I. Kozlov, and A. I. Lebedev, Phys. Lett. 38B, 129 (1972).